

A morphological study of galaxies in ZwCl0024+1652, a galaxy cluster at redshift $z \sim 0.4$

Zeleke Beyoro Amado^{1,2★}, Mirjana Pović^{1,3}, Miguel Sánchez-Portal^{4,5,6},
S. B. Tessema¹, Ángel Bongiovanni^{7,8,9}, Jordi Cepa^{7,8,9},
Miguel Cerviño¹⁰, J. Ignacio González-Serrano¹¹, Jakub Nadolny^{7,8},
Ana Maria Pérez García¹², Ricardo Pérez-Martínez¹³ and Irene Pintos-Castro¹⁴

¹*Ethiopian Space Science and Technology Institute (ESSTI), Entoto Observatory and Research centre (EORC),
Astronomy and Astrophysics Research and Development Division, P.O.Box 33679, Addis Ababa, Ethiopia*

²*Kotebe Metropolitan University, College of Natural and Computational Sciences, Department of Physics,
P.O.Box 31248, Addis Ababa, Ethiopia*

³*Instituto de Astrofísica de Andalucía (IAA-CSIC), Glorieta de la Astronomía s/n, 18008, Granada, Spain*

⁴*Instituto de Radioastronomía Milimétrica, Av. Divina Pastora 7, Núcleo Central, E-18012 Granada, Spain*

⁵*European Southern Observatory, Alonso de Córdova 3107, Vitacura, Santiago 763-0355, Chile*

⁶*Joint ALMA Observatory, Alonso de Córdova, 3107, Vitacura, Santiago 763-0355, Chile*

⁷*Instituto de Astrofísica de Canarias (IAC), E-38200 La Laguna, Tenerife, Spain*

⁸*Departamento de Astrofísica, Universidad de La Laguna (ULL), E-38205 La Laguna, Tenerife, Spain*

⁹*Asociación Astrofísica para la Promoción de la Investigación, Instrumentación y su Desarrollo, ASPID,
E-38205 La Laguna, Tenerife, Spain*

¹⁰*Centro de Astrobiología (CSIC/INTA), 28850 Torrejón de Ardoz, Madrid, Spain*

¹¹*Instituto de Física de Cantabria (CSIC - Universidad de Cantabria), Avda. de los Castros s/n, E-39005, Santander, Spain*

¹²*Centro de Astrobiología (CSIC/INTA), ESAC Campus, Camino Bajo del Castillo s/n, E-28692, Villanueva de la Cañada, Spain*

¹³*ISDEFE for ESA. Camino Bajo del Castillo s/n. Urb. Villafranca del Castillo. E-28692, Villanueva de la Cañada, Spain*

¹⁴*Department of Astronomy & Astrophysics, University of Toronto, 50 St. George Street, Toronto, ON M5S 3H4, Canada*

Accepted 2019 February 7. Received 2019 February 7; in original form 2018 November 25

ABSTRACT

The well-known cluster of galaxies ZwCl0024+1652 at $z \sim 0.4$, lacks an in-depth morphological classification of its central region. While previous studies provide a visual classification of a patched area, we used the public code called galaxy Support Vector Machine (galSVM) and HST/ACS data as well as WFP2 master catalogue to automatically classify all cluster members up to 1 Mpc. galSVM analyses galaxy morphologies through Support Vector Machine (SVM). From the 231 cluster galaxies, we classified 97 as early-types (ET) and 83 as late-types (LT). The remaining 51 stayed unclassified (or undecided, UD). By cross-matching our results with the existing visual classification, we found an agreement of 81%. In addition to previous Zwcl0024 morphological classifications, 121 of our galaxies were classified for the first time in this work. In addition, we tested the location of classified galaxies on the standard morphological diagrams, colour-colour and colour-magnitude diagrams. Out of all cluster members, $\sim 20\%$ are emission line galaxies (ELG), taking into account previous GLACE results. We have verified that the ET fraction is slightly higher near the cluster core and decreases with the clustercentric distance, while the opposite trend has been observed for LT galaxies. We found higher fraction of ET (54 %) than LT (46 %) throughout the analysed central region, as expected. In addition, we analysed the correlation between the five morphological parameters (Abraham concentration, Bershadsky-Concelice concentration, Asymmetry, Gini and M20 moment of light) and clustercentric distance, without finding a clear trend. Finally, as a result of our work, the morphological catalogue of 231 galaxies containing all the measured parameters and the final classification is available in the electronic form of this paper.

Key words: ZwCl0024+1652 – galaxy – cluster – Morphology – Early-Type – Late-Type – galSVM–Morphological fraction

1 INTRODUCTION

A consolidated observational fact is the outstanding difference in the properties of galaxies located in the cores (or regions of high local galaxy density) and in the external parts (or low density ones) of low- and intermediate- redshift clusters: the former regions are dominated by red, massive and passive early-type galaxies (ET galaxies, comprising elliptical and S0), while a substantial increase of the fraction of late-type galaxies (LT, comprising spiral and irregular objects) is observed in the latter. This was early identified by Zwicky (1942), and quantified by Dressler (1980) in the so-called morphology-density relation linking the increasing fraction of ET galaxies with local galaxy density. Similarly, a decrease of the fraction of star forming (SF) galaxies is observed with increasing local galaxy density (the SF-density relation, see for instance Pintos-Castro et al. 2013, and references therein). Moreover, these relations evolve with cosmic time, as was realized by Butcher & Oemler (1978), who found that cluster galaxy populations evolve as redshift changes in such a way that rich clusters at higher redshift ($z > 0.2$) are populated with a higher fraction of blue galaxies than low redshift clusters. This is the so-called Butcher-Oemler (BO) effect. Likewise, an increase of the cluster SF and active galactic nuclei (AGN) activity is observed (see for instance Haines et al. 2009; Martini et al. 2013).

The morphology-density relation seems to hold from nearby clusters up to redshifts as high as $z \sim 1.5$ (e.g. Dressler et al. 1997; Postman et al. 2005; Holden et al. 2007; Mei et al. 2012; Nantais et al. 2013). Likewise, star formation takes place in low density regions where LTs dominate while high density regions are dominated by quiescent ET galaxies since $z \sim 1.5$ to the local universe (e.g. Postman & Geller 1984; Kauffmann et al. 2004; Cooper et al. 2012; Wetzel et al. 2012; Woo et al. 2013). At higher redshift, there is some controversial evidence of the existence of a reversal of the SF-density relation: some authors, as Tran et al. (2010) find an (even dramatic) increase of the fraction of SF galaxies from low- to high-density regions in clusters at $z \sim 1.6$, while other authors (e.g. Ziparo et al. 2014) do not find a clear evidence of such type of reversal when studying clusters at the same redshift. Quadri et al. (2012), using mass-selected samples from the UKIDSS Ultra-Deep Survey, conclude that galaxies with quenched SF tend to reside in dense environments out to at least $z \sim 1.8$.

The structural and morphological properties of a galaxy are important tracers of its evolutionary stage. Thus, the correlation of the morphology (and/or SF activity) of the clusters' galaxies with the local density provides valuable information on the stage of infall at which galaxies experience the bulk of their transformations. To this end, it is important to perform wide-area surveys (to study the density-dependent effects) in clusters that span a range of redshifts (to assess the evolution with cosmic time).

The morphological taxonomy of galaxies can be backdated to Reynolds (1920). Visual inspection is the traditional method, and even now a very common way to perform morphological classification of galaxies (e.g. Lintott et al. 2008; Nair & Abraham 2010; Fasano et al. 2012; Kocovski et al. 2012; Kartaltepe et al. 2012, 2015; Buttrago et al. 2013; Kuminski & Shamir 2016; Willett et al. 2013; Simons et al. 2017; Willett et al. 2017). One of the drawbacks

of the visual classification method is the subjectivity, that can be alleviated by performing multiple instances of the classification of each object carried out by different persons; an outstanding example is Galaxy Zoo project (Lintott et al. 2008, 2011). In the framework of this “citizen science” initiative, nearly one million galaxies from the Sloan Digital Sky Survey (SDSS) were classified by $\sim 10^5$ participants who performed more than 4×10^7 classifications. Needless to say, when dealing with large number of sources, the visual classification method can be really time-consuming. It works well for closer and well resolved objects for accurate estimation. For such objects it agrees with the results of modern classification methods.

But with a currently overgrowing observational astronomical data, the above method is probably not the most appropriate or even unfeasible for high-redshift galaxies. Modern classification techniques include galaxy fitting algorithms, which can give reliable results for a large number of galaxies in a relatively shorter period and with minimal human resources. To deal with fast growing and big astronomical data, machine learning techniques employing Convolutional Neural Networks (CNN) are widely under use recently for morphological classification of galaxies (e.g. Banerji et al. 2010; Kuminski et al. 2014; Dieleman, Willett & Dambre 2015; Huertas-Company et al. 2015; Aniyani & Thorat 2017; Domínguez et al. 2018; Lukic et al. 2018). Modern galaxy classification methods can either be *parametric* or *non-parametric*.

Parametric methods use some parameters of the galaxies to classify them by fitting (one or two dimensional) mathematical models to their images assuming some predefined parametric model. In this approach Sérsic profile (Sérsic 1963) and a two-component profile (bulge + disk decomposition) are the commonly used models. The classification is obtained by fitting a two component profile as described in detail by Simard et al. (2002) and Peng et al. (2002). More recently, Simard et al. (2011) has performed a classification of 1.12 million galaxies using a bulge + disk decomposition approach with SDSS data release seven (Abazajian et al. 2009). In addition to this, a structural and morphological catalogue of 45 million sources have been presented by Tarsitano et al. (2018) with the Dark Energy Survey (The DES Collaboration 2016) data of the first year observation employing both a single Sérsic parametric fits and non-parametric methods. Parametric method in general is useful in that it gives a complete set of parameters describing the quantitative morphology. Since a large number of parameters need to be fitted, the results may be degenerated as shown in Huertas-Company et al. (2007). Degeneracy occurs as a result of correlation between parameters, the results of the local minima in the parameter space of the chi-square minimization, or by numerical divergence in the process of fitting (Peng et al. 2002, 2010). The peculiar characteristic of the parametric method in general is the assumption that a galaxy is described well by a simple analytic model whereas this does not always work for well resolved as well as irregular and merging/interacting galaxies.

On the other hand, the *non-parametric* approach does not assume any specific analytic model and is performed on the basis of measuring a set of well-chosen observables. The effects of seeing, being one of the major challenges in galaxy fitting, are not included in non-parametric mea-

measurements unlike the parametric ones where the assumed mathematical model is convolved with the PSF. The non-parametric method was introduced for the first time by Abraham et al. (1994, 1996) with the definition of two observables: the Abraham concentration index and asymmetry. A third quantity, namely smoothness, was introduced by Conselice et al. (2000, 2003). The classification has been further enhanced with additional observables: the GINI coefficient (Abraham et al. 2003); M20 moment of light (Lotz et al. 2004) and Conselice-Bershady concentration (Conselice et al. 2000; Bershady et al. 2000). These six parameters, together with ellipticity are described in more details in sub-section 3.3. *Non-parametric* methods are in advantage when classifying large sample of galaxies at higher redshifts, when lower resolution data are available (e.g. Scarlata et al. 2007; Tasca et al. 2009; Pović et al. 2009, 2013, 2015; Pintos-Castro et al. 2016). Furthermore, no analytic predefined profile is required in this approach.

In this paper, we apply a *non-parametric* classification method to a well-known intermediate redshift cluster, namely ZwCl0024+1652 at $z = 0.395$. This cluster has been extensively studied by several groups (e.g. Morrison et al. 1997; Broadhurst et al. 2000; Kneib et al. 2003; Treu et al. 2003; Moran et al. 2007; Geach et al. 2009; Natarajan et al. 2009; Sánchez-Portal et al. 2015). In particular, it has been observed by our team in the framework of the GaLAXy Cluster Evolution Survey (GLACE; Sánchez-Portal et al. 2015) in the H α and [NII] emission lines to trace the SF and AGN activity in a wide range of environments (see Sect. 5 below). Although this cluster has been deeply studied in some aspects, a visual morphological classifications has been performed for a limited number (214) of member galaxies within a clustercentric distance extending to 5 Mpc (Moran et al. 2007). The purpose of this work is to improve the knowledge about the morphological properties of the member galaxies by providing a reliable classification of the sources up to 1 Mpc of clustercentric radius. We use publicly available Hubble Space Telescope (HST) Advance Camera for Survey (ACS) data in F775W filter.

Only 66 galaxies have been classified by Moran et al. (2007) within this radius ($\approx 31\%$ of the total sample). Second important objective of this work is to compare visual classification of Moran et al. (2007) with our *non-parametric* method - this may provide us with handy-tool for future works at higher redshifts.

In our present work, we use a *non-parametric* method called galSVM introduced by Huertas-Company et al. (2008). galSVM fits a number of parameters simultaneously and assigns probabilities for each galaxy to be classified. Then based on the probabilities, the galaxies are classified into two broad morphological classes, namely early-type (ET) and late-type (LT). For more details about this classification, we refer the reader to Section 3.5.

The paper is organized as follows: Section 2 describes the data, along with a brief description of the generated source catalogue. In Section 3 the galSVM code and its application to our sample are described. The analysis on the results from our classification are further developed in Section 4. A detailed discussion is presented in Section 5. Finally Section 6 presents brief conclusions of this work.

The following cosmological parameters are assumed throughout this paper: $\Omega_M = 0.3$, $\Omega_\Lambda = 0.7$, $\Omega_k = 0$ and

$H_0 = 70 \text{ Kms}^{-1} \text{ Mpc}^{-1}$. All magnitudes are given in AB system as described by Oke & Gunn (1983), unless otherwise stated.

2 DATA

2.1 HST/ACS data

We used the public HST reduced scientific image of ZwCl0024+1652¹ from the observation made on 16 November 2004 with the ACS Wide Field Camera (WFC) using the F775W filter. The ACS/WFC has a pixel scale of $0.05 \text{ arcsec/pixel}$ and field of view of $202 \times 202 \text{ arcsec}^2$. The cluster is centred at RA = 6.64433 deg and DEC = 17.16211 deg, and the used image covers the central part of cluster of $\sim 1 \text{ Mpc}$. The image data is shown in Fig. 1 with all the sources labeled.

2.2 WFP2 supercatalogue data

To extract redshift information and to identify cluster members, we used the public ZwCl0024+1652 master catalogue² described in Treu et al. (2003) and Moran et al. (2005). The catalogue consists of 73,318 sources, with photometric and/or spectroscopically confirmed redshifts available, and covering the area of $0.5 \times 0.5 \text{ deg}^2$ up to the clustercentric distance of about 5 Mpc. All observations were carried out with the Canada-France-Hawaii Telescope (CFHT) and its CFH12K wide field camera, and/or the HST Wide Field and Planetary Camera (WFP2), as described in Treu et al. (2003). Beside redshifts, this catalogue includes the visual morphological classification of sources brighter than $I = 22.5$ (Moran et al. 2005). We cross-matched this catalogue with our SExtractor catalogue (3515 sources) using a maximum radius of 2 arcsec. This radius was selected after testing different ones from 1 to 5 arcsec and finding it to be the best compromise between being the counterparts and having multiple matches. We obtained a total of 255 counterparts (hereafter cluster sample) with available redshifts. In total, 126 and 129 sources have spectroscopic and photometric redshift measurements. The redshift distribution of the members is given in Fig. 2, including spectroscopic and photometric measurements.

3 MORPHOLOGICAL CLASSIFICATION

In this section we describe the morphological classification of the ZwCl0024+1652 cluster galaxies in detail. We first go briefly through the methodology used, obtained results, and final classification.

¹ Based on observations made with the NASA/ESA HST, and obtained from the Hubble Legacy Archive, which is a collaboration between the Space Telescope Science Institute (STScI/NASA), the Space Telescope European Coordinating Facility (ST-ECF/ESA) and the Canadian Astronomy Data centre (CADAC/NRC/CSA)

² <http://www.astro.caltech.edu/~smm/clusters/>

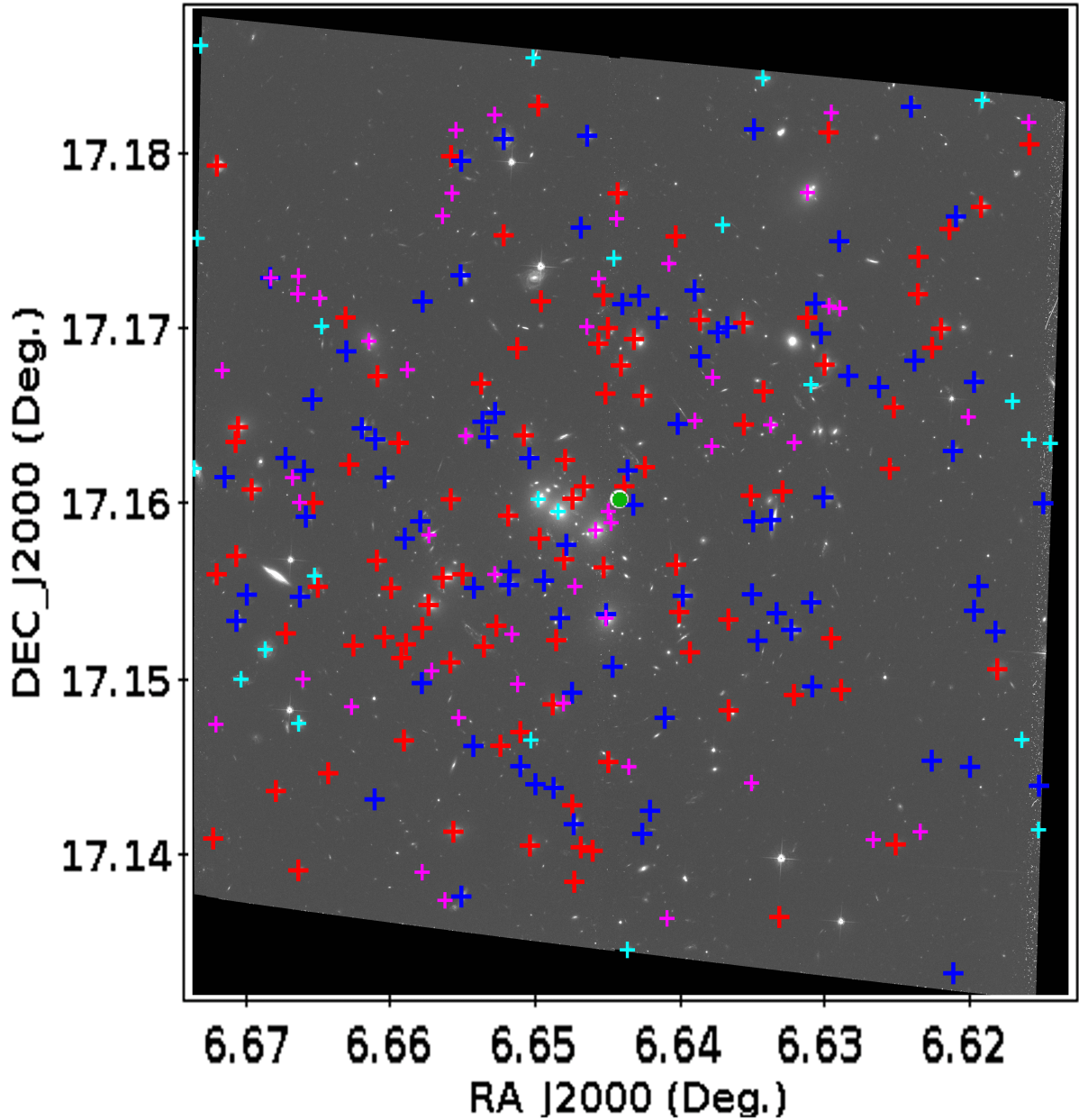


Figure 1. The ACS/WFC image of ZwCl0024+1652 galaxy cluster used in this work, where east is to the left and north at the top. The centre of the cluster is indicated by a large green dot. The larger red and blue crosses indicate galaxies classified as ET and LT, respectively. While the smaller cyan crosses show those galaxies for which the probabilities are not measured and the magenta crosses show galaxies with measured probabilities but undecided morphologies (see Sec. 3).

3.1 Methodology

In this work we use galSVM (Huertas-Company et al. 2008) to classify galaxies morphologically in the ZwCl0024+1652 cluster. The galSVM is a public code that uses a free library libSVM (Chang & Lin 2011) and works in IDL environment. It has been successfully tested previously, at different redshifts, and on both field and cluster galaxies (e.g., Huertas-Company et al. 2009, 2010, 2011; Pović et al. 2012, 2013, 2015; Pintos-Castro et al. 2016).

For source detection, flux extraction, and measurement of the morphological parameters we need for the morphologi-

cal classification (e.g., ellipticity), we run SExtractor (Bertin & Arnouts 1996). We extracted 3515 possible sources, including cluster members and field galaxies. galSVM uses local sample with known visual morphologies (see Sec. 3.2) and use it to learn how these may be seen at redshifts and magnitudes distributions of our real sample. It consists of several steps. First, it simulates local galaxies, by placing them to the redshift and magnitude distributions characteristic of the real sample. Secondly, it drops simulated local galaxies into the background that corresponds to the real sample image. Third, it measures different morphological

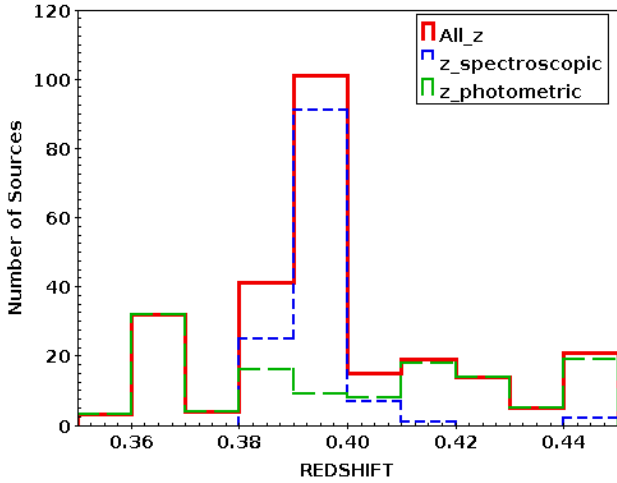


Figure 2. Redshift distribution of our real ZwCl0024+1652 sample where the red solid lines stands for the total sample, the blue dashed lines for spectroscopic redshifts and the dashed green lines for photometric redshifts.

parameters (see Sec. 3.3), first of the simulated local sample, and then of the real sample of galaxies that we want to classify. Finally, it compares morphological parameters of the training simulated local galaxies with their known visual classification, and determines conditions inside the multiple-parameters space that are then applied to the real sample to be classified. The final classification is based on a number of Montecarlo (MC) simulations, where each simulation gives a probability that the galaxy is early-type (ET). The average probability (P_{avg}) and measured error give the final classification that the galaxy is ET. The probability that galaxy is late-type (LT) will then be $1 - P_{avg}$. For more details regarding galSVM see Huertas-Company et al. (2008). For applying galSVM, to include morphology determination for more fainter galaxies we took a magnitude limit of $F775W \leq 26$.

3.2 Training sample of local galaxies

We used a catalogue of 3000 visually classified local galaxies, with known redshifts and magnitudes. The sample was selected randomly from the Nair & Abraham (2010) catalogue of visual morphology consisting of about 14000 galaxies taken from the Sloan Digital Sky Survey (SDSS)³ DR4 data. The redshift distribution of our local sample is in a

range of 0.01-0.1, and most of galaxies are bright with r band magnitude between 13 and 17. The magnitude and redshift distributions of the training sample versus that of the real data are shown in the two plots of Fig. 3. The detailed description of the training sample can be found in Pović et al. (2013). The training sample of 3000 local galaxies was selected as a good compromise between the computing time and accuracy in classification (both being highly sensitive to the training sample size). In addition, equal number of ET and LT galaxies were taken into account to obtain more precise morphology, and the selected sample can be considered as representative of the whole data with respect to general galaxy properties, as shown in Pović et al. (2013).

3.3 Measured morphological parameters

We used the following six parameters simultaneously to run galSVM: ellipticity (obtained by SExtractor), asymmetry, Abraham concentration index, GINI coefficient, M20 moment of light, and Conselice-Bershady concentration index. The last five were measured using galSVM and are briefly described as follows.

- (i) **Asymmetry (ASYM)**, measures an extent to which galaxy's light is rotationally symmetric (Abraham et al. 1994, 1996; Conselice et al. 2003).
- (ii) **Abraham concentration index (CABR)**, is defined as the ratio of fluxes of the inner isophote at 30 % to that of the outer isophote at 90 % (Abraham et al. 1994, 1996).
- (iii) **GINI coefficient (GINI)**, is a statistical term derived from the Lorentz curve specifying the overall distribution function of the pixel values of the galaxy (Abraham et al. 2003; Lotz et al. 2004).
- (iv) **M20 Moment of light**, describes the second order normalized moment of the 20 % brightest pixels of the particular galaxy (Abraham et al. 2003; Lotz et al. 2004).
- (v) **Bershady-Conselice concentration index (CCON)**, measures a light ratio within a circular inner aperture (radii comprising of 20 % of the total flux) to the outer aperture (radii containing 80 % of the total flux) of the galaxy (Conselice et al. 2000; Bershady et al. 2000; Conselice et al. 2003).

In all measurements, the total flux is defined as the amount of flux contained within 1.5 times the Petrosian radius, where the Petrosian radius was measured with SExtractor. The centre of the galaxy is defined by minimizing ASYM index. More details on all parameters can be found in Huertas-Company et al. (2008) and Pović et al. (2013).

3.4 galSVM applied to ZwCl0024+1652

To measure the morphologies of ZwCl0024+1652 cluster members, we run galSVM on the HST/ACS F775W image described in Sec. 2.1, and used the SExtractor catalogue of 255 sources with all needed input parameters and redshifts available (see Sec. 2.1 and 2.2). We went through all

³ SDSS is managed by the Astrophysical Research Consortium for the Participating Institutions of the SDSS Collaboration including the University of Arizona, the Brazilian Participation Group, Brookhaven National Laboratory, Carnegie Mellon University, University of Florida, the French Participation Group, the German Participation Group, Harvard University, the Instituto de Astrofísica de Canarias, the Michigan State/Notre Dame/JINA Participation Group, Johns Hopkins University, Lawrence Berkeley National Laboratory, Max Planck Institute for Astrophysics, Max Planck Institute for Extraterrestrial Physics, New Mexico State University, New York University, Ohio State University, Pennsylvania State University, University of Portsmouth, Princeton University, the Spanish Participation Group, University of

Tokyo, University of Utah, Vanderbilt University, University of Virginia, University of Washington, and Yale University.

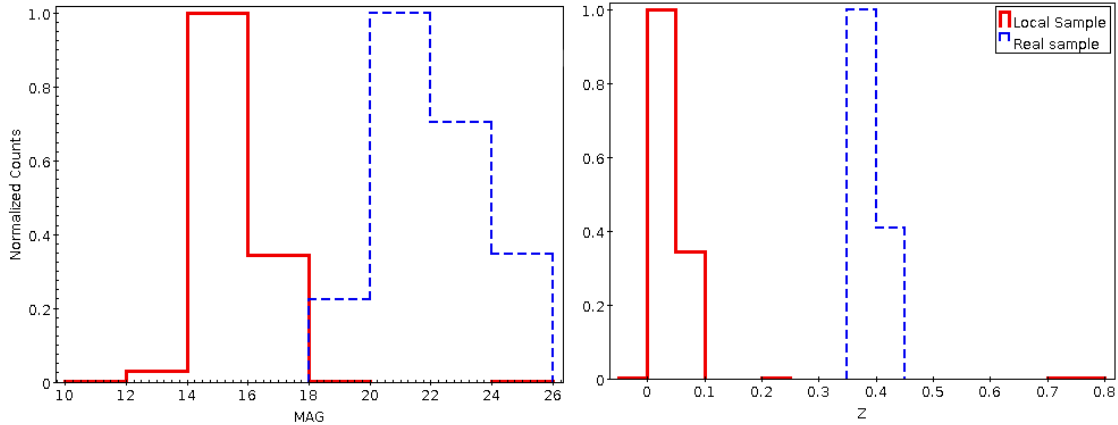


Figure 3. Magnitude (*right plot*) and redshift (*left plot*) distributions of the local training sample with known morphology (red solid lines) and the real ZwCl0024+1652 sample that should be classified (blue dashed lines).

galSVM steps described in Sec. 3.1, using the 3000 SDSS local galaxies as a training sample (see Sec. 3.2). We measured all parameters described in Sec. 3.3 of both training and real samples. For final classification we run 15 MC simulations, where in each simulation we used 2000 different randomly selected local galaxies (out of 3000) with the same number of ETs and LTs. The number of MC simulations was selected as the best compromise between the computational time and accuracy of results (see Pović et al. 2013).

Taking into account previous results obtained in Pović et al. (2013), dividing a sample into different magnitude ranges can increase the accuracy of morphological classification by optimizing the galSVM code for fainter galaxies. Therefore in this work we run galSVM three times, using the following ranges.

- (i) $F775W \leq 22.0$ (137 galaxies),
- (ii) $22.0 < F775W \leq 24.0$ (216 galaxies), and
- (iii) $F775W \leq 26.0$ (255 galaxies).

For each range we provided the corresponding magnitude and redshift distributions of cluster members for simulating during the classification process. These distributions are shown in Fig. 4 for both training sample after being simulated and the real sample to be classified. For the final classification we follow the findings of Pović et al. (2013), and considered the results from the first magnitude bin, from the second, but only for those sources not present in the first one (for $22.0 < \text{MAG_AUTO} \leq 24.0$), and finally from the third bin, but only for those sources not present in the previous two (for $24.0 < \text{MAG_AUTO} \leq 26.0$).

3.5 Final classification

In all galSVM runs (i.e. for each magnitude bin) we obtain a final average probability from 15 MC simulations (for more details about the training sample and the running setup see Sections 3.2 and 3.4). Finally, we obtained PROBA_AVG⁴ with corresponding uncertainty values for 231 galaxies out of 255. For the remaining 24 galaxies, PROBA_AVG was not measured either because one or more parameters have values

Table 1. The PROBA_FINAL values in the three magnitude ranges

	Median	[Q1 - Q3]
$F775W \leq 22.0$	0.745	0.263 - 0.877
$22.0 < F775W \leq 24.0$	0.474	0.170 - 0.727
$24.0 < F775W \leq 26.0$	0.478	0.271 - 0.569

Table 2. The PROBA_ERR values in the three magnitude ranges

	Median	[Q1 - Q3]
$F775W \leq 22.0$	0.044	0.030 - 0.067
$22.0 < F775W \leq 24.0$	0.045	0.032 - 0.059
$24.0 < F775W \leq 26.0$	0.069	0.054 - 0.122

out of the respective standard range (Huertas-Company et al. 2008), or they simply were not measured by galSVM. Of these, 50 % are located on image borders, while most of the remaining sources are merging/interacting systems or some are edge on galaxies. Only 3 galaxies (out of 24) have close companions, but the sample is not statistically significant for doing any additional studies. Tables 1 and 2 give the median values and Q1 to Q3 ranges⁵ of average probability [Q1 - Q3]⁶ and its error in three magnitude bins. It can be seen that most of the brightest galaxies ($F775W \leq 22.0$) are characterized by larger probability (median value > 0.7) to be ETs, while for fainter galaxies (2nd and 3rd bin) probability to be ET is lower than 0.5. As we could expect, the error values increase for fainter bins (see Table 2).

For the final classification we took into account the measured errors and considered a galaxy to be ET if $\text{PROBA_FINAL} = \text{PROBA_AVG} \pm \text{PROBA_ERR} > 0.6$ (or 0.7 in the last magnitude bin), and to be LT if $\text{PROBA_FINAL} < 0.4$ (or 0.35 in the last magnitude bin),

⁵ Q1 stands for quartile1 (25% of the sample) and Q3 for quartile3 (75% of the sample)

⁶ [Q1 - Q3] stands for the range of values characteristic of 50% of the analysed sample

⁴ PROBA_AVG is average probability measured by galSVM

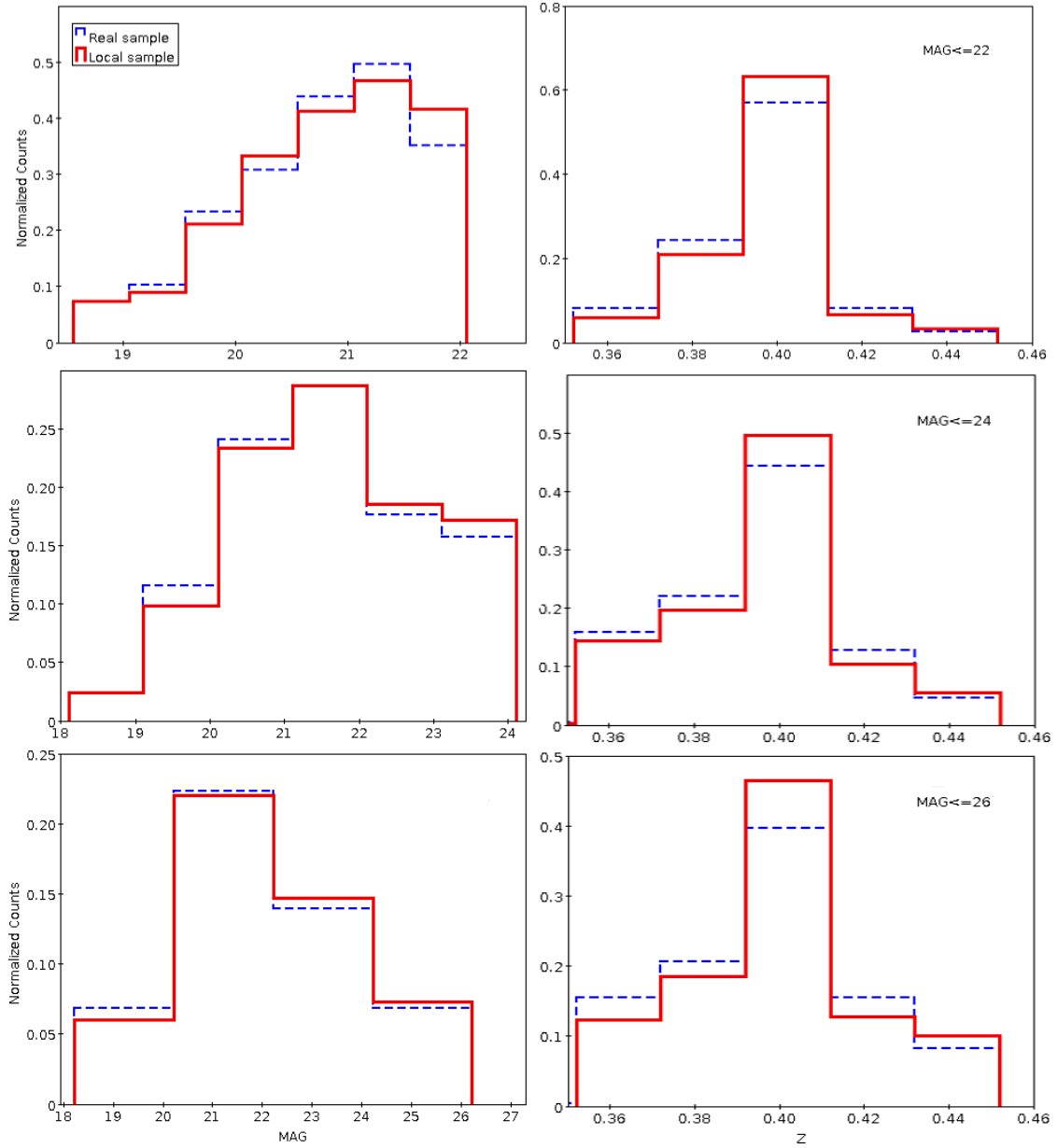


Figure 4. Magnitude (*left plots*) and redshift (*right plots*) distributions of our real data (blue dashed lines) and the simulated local sample (red solid lines). The distributions are plotted for $F775W \leq 22.0$ (top plots), $F775W \leq 24.0$ (middle plots), and $F775W \leq 26.0$ (bottom plots).

where PROBA_ERR is uncertainty in measuring probability and PROBA_FINAL is the final probability after error correction. For those galaxies with $0.4 < \text{PROBA_FINAL} < 0.6$ (or between 0.35 and 0.7 in the last magnitude bin) we are not able to classify them morphologically, and they will remain inside the ‘undecided class’ (UD). To define the classification boundaries, we used previous works of Pović et al. (2012, 2013) and Pintos-Castro et al. (2016). Fig. 5 shows the PROBA_FINAL distributions in the three magnitude ranges, while the final classification is summarized in Table 3. As can be seen, out of a total of 231 galaxies with measured final probabilities, we have 97 (42%), 83 (36%), and 51 (22%) galaxies classified as ET, LT, and UD, respectively. Figure 6 shows the PROBA_FINAL of the whole clas-

sified sample. We marked in Fig. 1 all the classified sources with red and blue crosses respectively for ET and LT galaxies respectively. Of the classified sources ET (LT) galaxies 59 (41) have spectroscopically confirmed and 38 (42) have photometric redshifts. Few bright galaxies (e.g. close to the cluster centre) remained unclassified, mainly due to the difficulty that galSVM had with classifying galaxies being in rich environments and with close companions. Moreover, it has also been deduced that only 21.6% of the UD galaxies have spectroscopically confirmed redshifts while for the classified ones (ET or LT), 62.2% have spectroscopic redshifts.

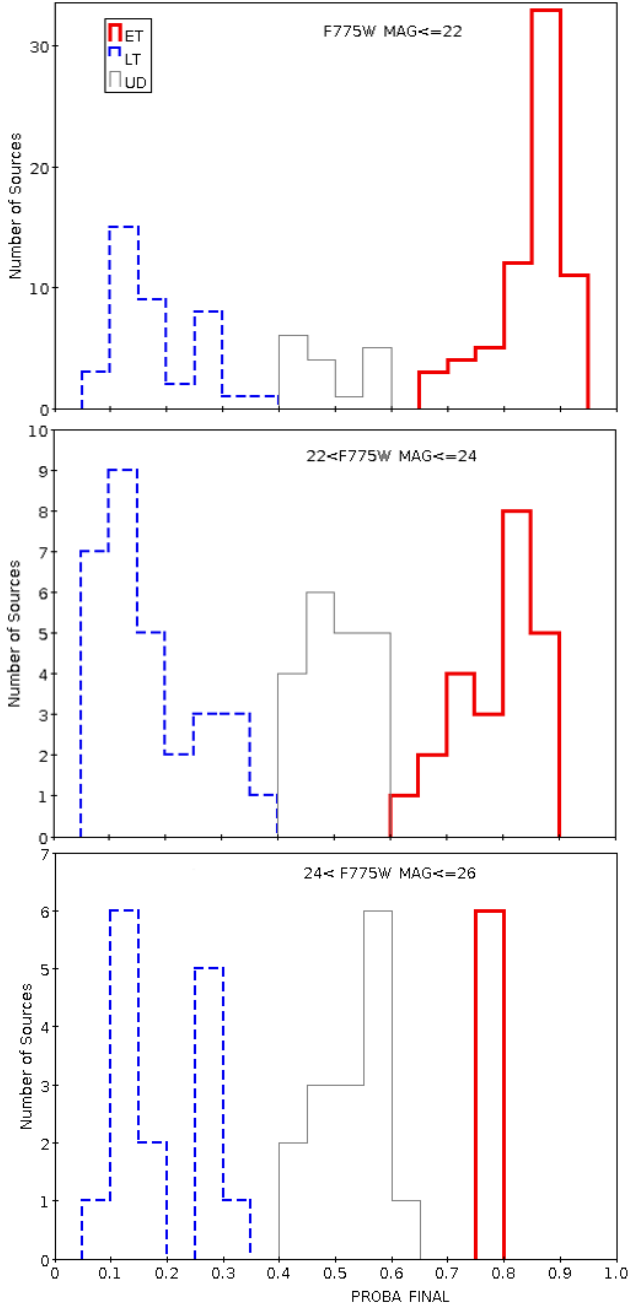


Figure 5. Final error corrected probability distributions of all galaxies classified as ET (red thick solid lines), LT (dashed blue lines), and UD (grey thin solid lines) in the three magnitude ranges.

4 ANALYSIS

4.1 Comparisons with visual morphological classification

The visual morphological classification of 214 galaxies with spectroscopically confirmed redshifts in ZwCl0024+1652 was carried out previously by [Moran et al. \(2007\)](#), covering the clustercentric distance of 5 Mpc. In this section we compare our non-parametric classification of 231 galaxies, within

Table 3. Final classification of the ZwCl0024+1652 cluster members.

	ET	LT	UD	Total
$F775W \leq 22.0$	68 (55%)	39 (32%)	16 (13%)	123
$22.0 < F775W \leq 24.0$	23 (32%)	29 (40%)	20 (28%)	72
$24.0 < F775W \leq 26.0$	6 (17%)	15 (42%)	15 (41%)	36
Total	97	83	51	231

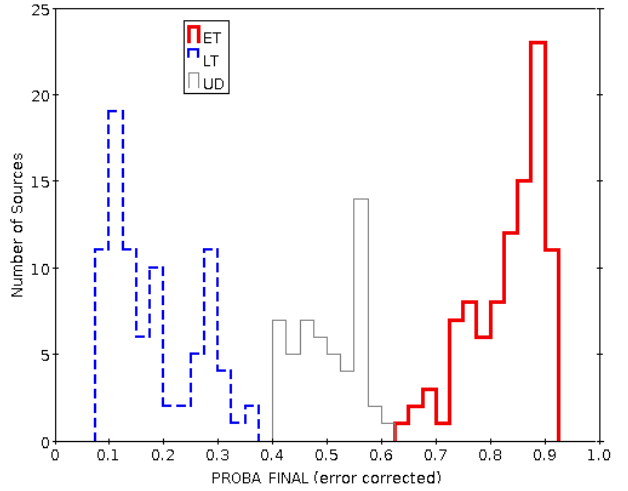


Figure 6. Final error corrected probability distributions of all ET (red thick solid lines), LT (dashed blue lines), and UD (grey thin solid lines).

the clustercentric distance of 1 Mpc (see Sec. 2), with the visual one. Within the region of our data (~ 1 Mpc radius) we determined that there are 123 sources with spectroscopically confirmed redshifts having visual morphology as in [Moran et al. \(2007\)](#). While in our sample catalogue with measured probabilities (231 sources) we have 111 sources with spectroscopic redshifts and 120 sources with photometric redshifts. We cross-matched the two catalogues using the radius of 2 arcsec, and found a total 66 counterparts. The reason of a small number of counterparts is mainly because of the fact that [Moran et al. \(2007\)](#) visual classification was done only for galaxies with confirmed spectroscopic redshifts and only considers the best resolved galaxies. The I-band magnitude limit of galaxies in [Moran et al. \(2007\)](#) is 22.3, with 201 (95%) of galaxies being brighter than $I = 22$, whereas our magnitude limit in F775W-band is 26. The L-band magnitude distribution comparison of both works is given in Fig. 7.

Out of 66 counterparts, 50 and 16 galaxies were classified visually by [Moran et al. \(2007\)](#) as ET and LT respectively. When compared with our results, 53 galaxies, or 81%, match the visual classification, of these 41 being classified as ET, and 12 as LT. Of the remaining 13 galaxies, 7 have visual classification available, but were classified as UD in our work, while for the other 6 galaxies ET/LT classification is in disagreement between the two works. Visually checking these galaxies, we found that 3 of them are edge on (S0 in [Moran et al. \(2007\)](#) while LT in our work possibly Sa that both could be possible). The other three galaxies were classified as ET in our work whereas 2 of them are Sa + b and

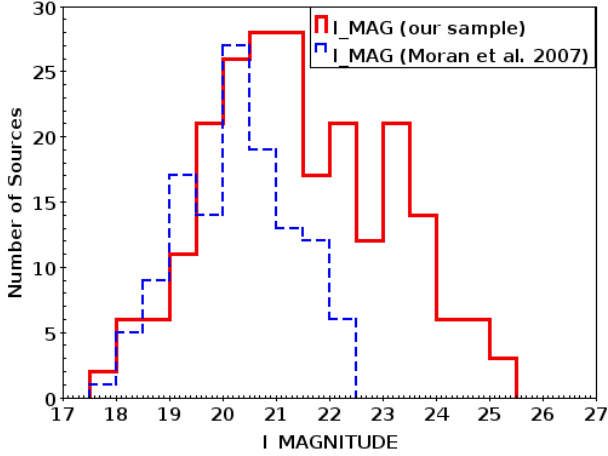


Figure 7. Comparison between the I band magnitude (red solid line) of our sample galaxies classified in this work using galSVM and the I band magnitude of the counterparts from Moran et al. (2007) visually classified cluster members (blue dashed line).

one is Sc + d in Moran et al. (2007); our classification being right for one while one is observed to be an interacting system and the remaining one is peculiar galaxy. Finally, after these comparisons we conclude that 81% of our classification is in a good agreement with the visual classification. Moreover, in this work we provide a reliable classification of additional 121 galaxies within 1 Mpc of clustercentric distance, being classified for the first time.

4.2 Morphological parameters

The distributions of different measured morphological parameters of 180 ET and LT classified cluster members are given in Fig. 8. In addition to the histograms, Table 4 summarizes the median values of each parameter and [Q1-Q3] range characteristic of cluster members classified as ET or LT. As can be seen from both Fig. 8 and Table 4, all parameters follow the expected trends of ET and LT galaxies, with concentration indices such as CABR, CCON and GINI being characterised with higher values in case of ETs, while ASYM, M20, and ELLIP are showing higher values for LTs. If we compare our results with those obtained by Pović et al. (2013), using the same methodology and data of the ALHAMBRA survey (Moles et al. 2008) in F613W band, ZwCl0024+1652 galaxies classified as ET seem to be slightly more concentrated (in terms of all concentration indices), and characterised with lower asymmetries in the case of both ET and LT.

4.3 Morphological diagnostic diagrams

In this section, we tested some of the commonly used morphological diagnostic diagrams by comparing the measured morphological parameters. Fig. 9 shows six different diagrams and relations between CABR and ASYM, GINI, and CCON (left plots, from top to bottom, respectively), and M20 and CCON, GINI, and CABR (right plots, from top to bottom, respectively). These relations have been used in many previous works, showing a separation between ET and LT galaxies (e.g., Abraham et al. 1994, 1996; Conselice et

Table 4. Median and [Q1 - Q3] range of measured morphological parameters of galaxies classified as ET or LT.

Parameter	Measure	ET	LT
CABR	median	0.493	0.322
	[Q1 - Q3]	0.430 - 0.532	0.268 - 0.374
CCON	median	8.894	6.865
	[Q1 - Q3]	8.265 - 9.548	6.020 - 7.470
GINI	median	0.650	0.534
	[Q1 - Q3]	0.614 - 0.694	0.452 - 0.587
ASYM	median	0.040	0.062
	[Q1 - Q3]	0.025 - 0.059	0.021 - 0.158
M20	median	-1.996	-1.597
	[Q1 - Q3]	-2.195 - -1.726	-1.805 - -1.401
ELLIP	median	0.224	0.433
	[Q1 - Q3]	0.102 - 0.307	0.303 - 0.585

al. 2000; Abraham et al. 2003; Conselice et al. 2003; Lotz et al. 2004; Cassata et al. 2007; Scarlata et al. 2007; Tasca et al. 2009; Pović et al. 2009, 2013; Pintos-Castro et al. 2016; Tarsitano et al. 2018).

It can be seen in all plots that ZwCl0024+1652 cluster members classified as ET and LT are occupying different areas on diagrams, as expected. ETs are located again in the regions characterised with higher concentrations (larger values of CABR, GINI, and CCON and lower of M20), in comparison to LTs. ASYM parameter is much more delicate in separating sources, as has been commented previously (Pović et al. 2015), and as can be seen in Fig. 9 (top left plot). However, it can be efficient in selecting interacting systems, showing larger values as can be seen in the same plot for sources with $ASYM > 0.5$. The relationships depicted are all in agreement with recent works (e.g. Castellón et al. 2014; Parekh et al. 2015; Pintos-Castro et al. 2016). We took into account studies of Tarsitano et al. (2018) and their Figure 11. We reproduced Gini vs. M20 diagram color coded with CABR, CCON, ASYM, and ELLIP finding the results in line with our Fig. 9.

4.4 Colour-colour and colour-magnitude relations

In this section we tested the colour-colour and colour-magnitude diagrams for ZwCl0024+1652 cluster members classified as ETs and LTs. These diagrams have been tested at both lower and higher redshifts, and it is very well known that the distribution of galaxies on them is bimodal, with ETs being mainly located in the red sequence and LTs in the blue cloud (e.g., Bell et al. 2003; Cassata et al. 2007; Melbourne et al. 2007; Pović et al. 2013; Schawinski et al. 2014, etc.). In Fig. 10 we represented the relation between the R - K versus B - R rest-frame colours (left plot), and between the B - R rest-frame colour and absolute magnitude in the B band (right plot). We also represent the histograms of all parameters used in the 2d plots, and their distributions for both ET and LT galaxies. In the two plots we can see the area with a higher density of ET sources, and that in general brighter and redder regions have higher fractions of ETs, as

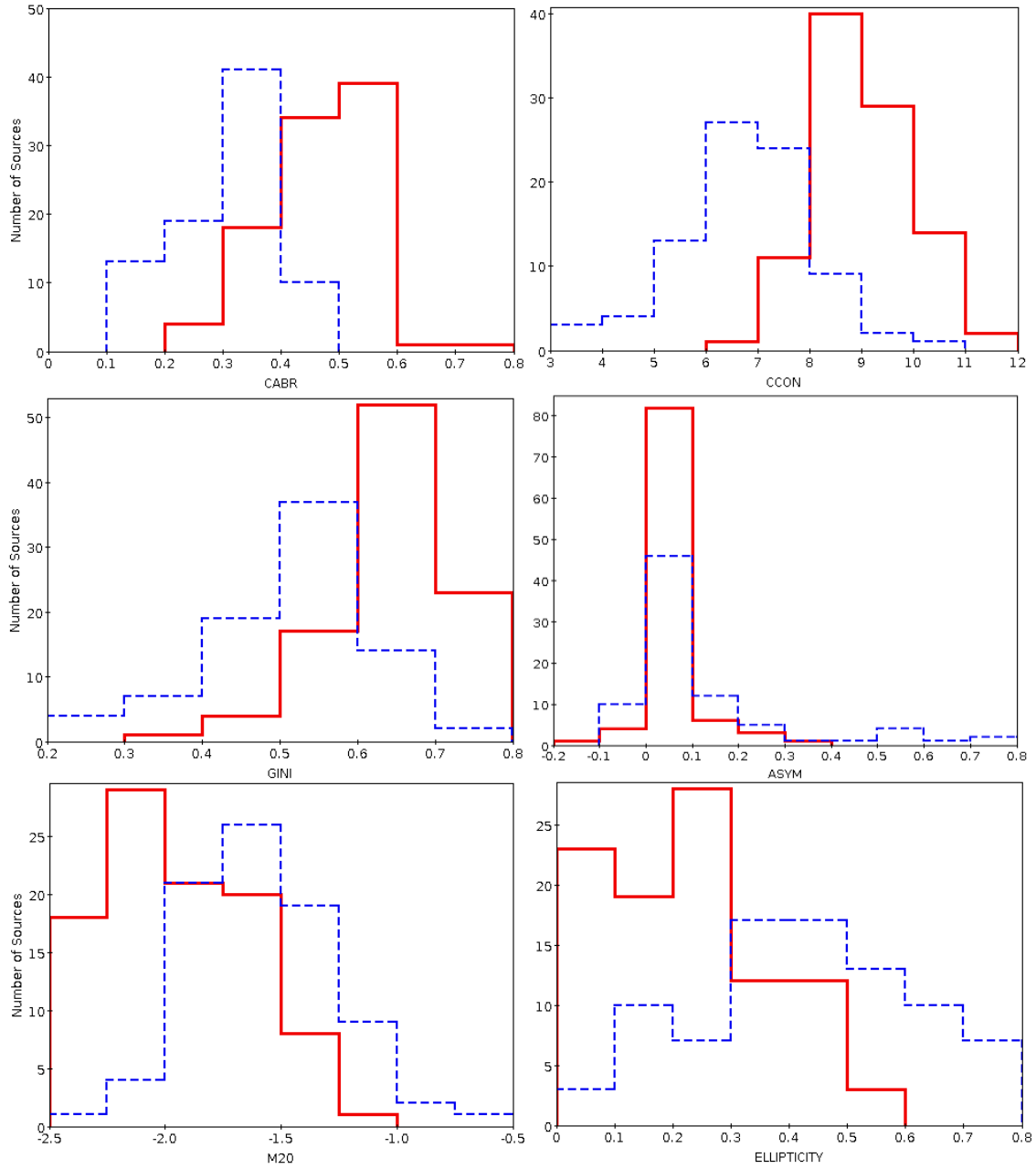


Figure 8. (From top left to bottom right:) Distributions of CABR, CCON, GINI, ASYM, M20 moment of light, and ellipticity parameters of ET (red solid lines) and LT (blue dashed lines) galaxies.

expected, while fainter and bluer parts of the diagram are populated more with LTs.

4.5 Morphology vs. clustercentric distance

The distance between member galaxy and the centre of the cluster is calculated using the spherical law of cosines as:

$$\cos(D_s) = \sin(\delta_c) \times \sin(\delta_g) + \cos(\delta_c) \times \cos(\delta_g) \times \cos(|\alpha_c - \alpha_g|), \quad (1)$$

where (α_c, δ_c) are right ascension and declination of the cluster centre in radians, while (α_g, δ_g) are galaxy coordinates.

To measure the clustercentric distance in Mpc, we used the following:

$$R = D_{cl} \times \tan(D_s) \approx D_{cl} \times D_s, \quad (2)$$

where $D_{cl} = 1500 \text{ Mpc}$ and is the distance to ZwCl0024+1652. Fig. 11 shows the distribution of clustercentric distance of 180 cluster members classified as ETs and LTs, while Table 5 provides the basic statistics (median and [Q1 - Q3] ranges) of both morphological types.

We also analysed the relation between the galaxy brightness, in terms of F775W magnitude and surface

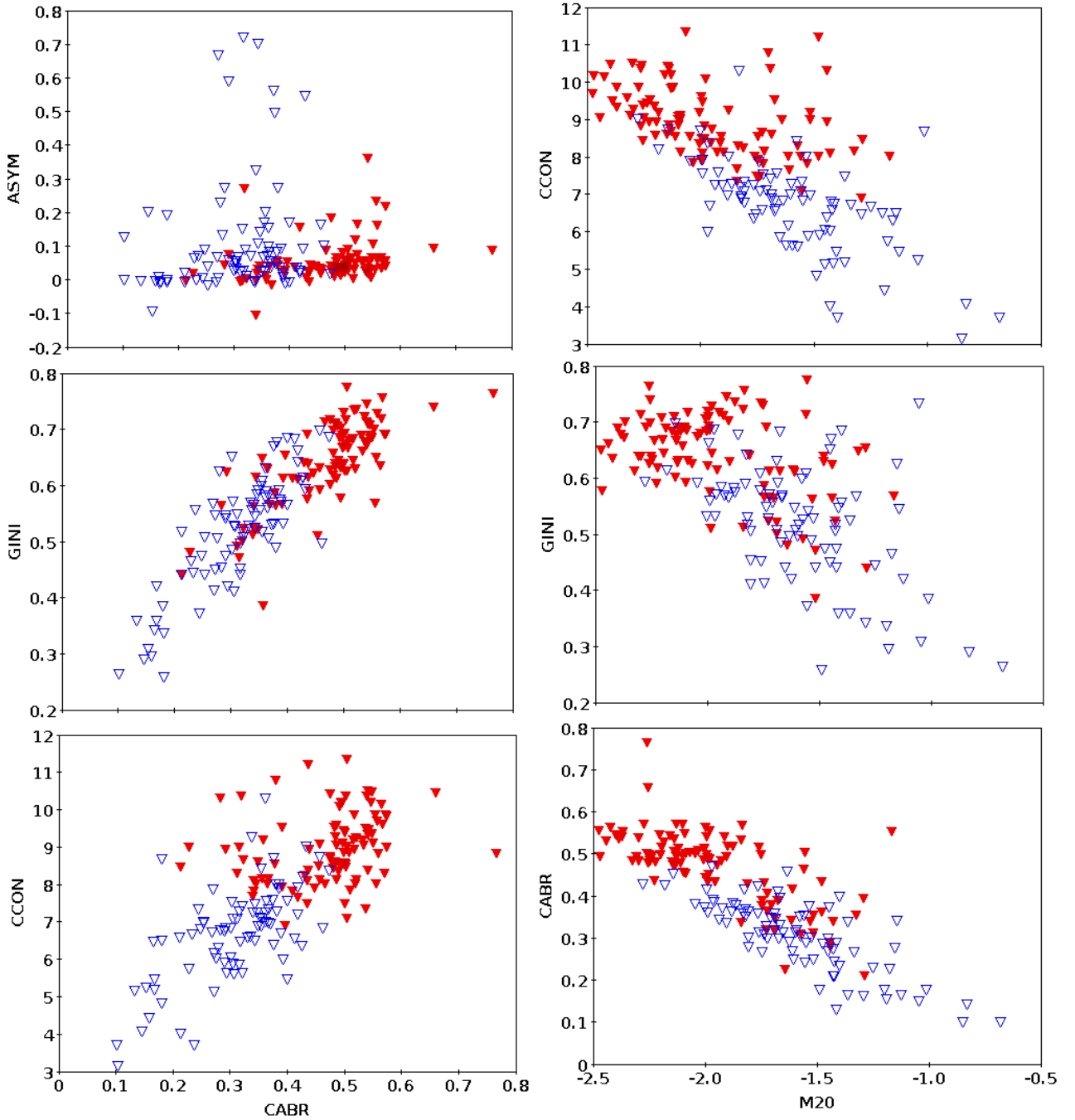


Figure 9. Standard morphological diagnostic diagrams showing the relation between CABR and ASYM, GINI, and CCON (left plots, from top to bottom, respectively), and M20 and CCON, GINI, and CABR (right plots, from top to bottom, respectively). In all the plots red solid and blue open triangles stand for ET and LT galaxies, respectively.

brightness (MUMEAN), and clustercentric distance, as shown in Fig. 12. For the two morphological types, Table 5 gives again the main statistics regarding the brightness.

Finally, we analysed the relation between the clustercentric distance (R) and morphological parameters measured in previous section. Fig. 14 shows for the first time for ZwCl0024+1652 how the six morphological parameters vary with respect to the clustercentric distance in the case of cluster members classified as ET and LT. We also selected

those sources classified as LTs in this work, and that taking into account previous studies of Parekh et al. (2015) and visual inspection seem to be mergers. We discussed all plots and statistics in Sec. 5.

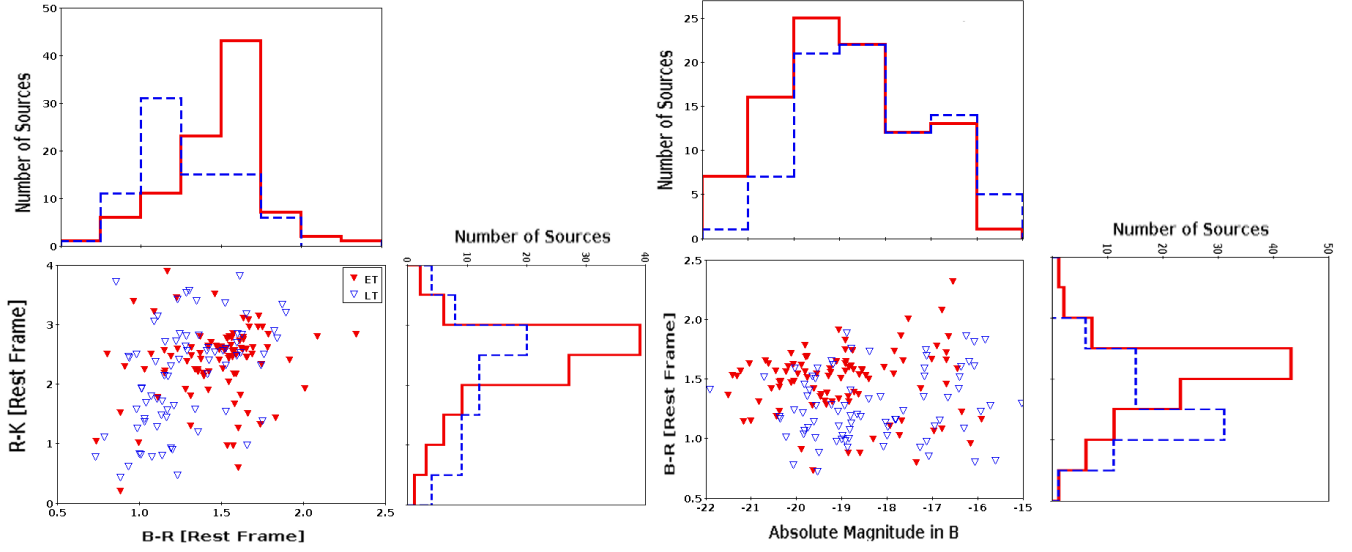


Figure 10. Rest frame R - K vs. B - R colour-colour diagram (left plot), and B - R rest-frame colour and absolute magnitude in B diagram (right plot)

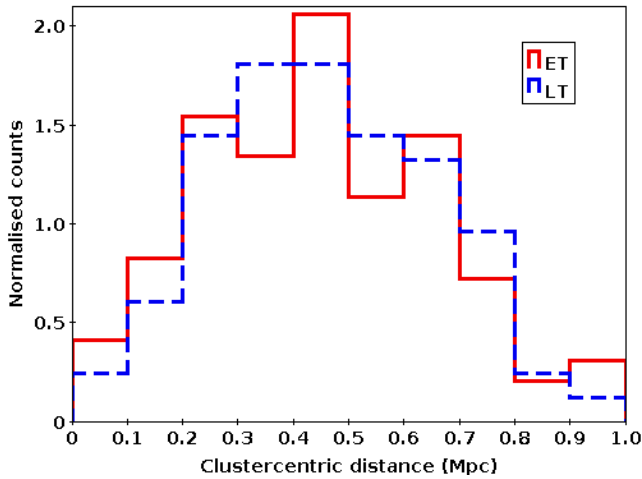


Figure 11. Normalised distribution of the clustercentric distance of galaxies classified as ET (red solid lines) and LT (blue dashed lines).

5 RESULTS AND DISCUSSION

5.1 Morphological classes

It was pointed out that the evolution of ET proportion is affected by redshift in addition to density and clustercentric distance (Smith et al. 2005; Postman et al. 2005; Simard et al. 2009). The BO effect (Butcher & Oemler 1984) verified with works for different redshift ranges, have been indifferently shown that LT proportion increases with redshift (e.g. Fairley et al. 2002 for $z \sim 0.2 - 0.5$, de Lucia et al. 2007 for $z \sim 0.4 - 0.8$, Barrena et al. 2012 for $z \sim 0.2 - 0.5$ and Castellón et al. 2014 for $z \sim 0.17 - 0.6$). These studies show that the proportion of LTs at $z \sim 0.4$ accounts about $\sim 35\% - 40\%$. In our current work the fraction of LT galaxies is $\sim 36\%$, which is in agreement with previous results.

Table 5. Statistical analysis of the morphological class distribution with respect to the clustercentric distance (R), the MUMEAN and the F775W_MAG values. Here the median and the value range [$Q1 - Q3$] for 50% of the sources in each class to fall is computed

Parameter	Measure	ET	LT
R	median	0.455	0.477
	[$Q1 - Q3$]	0.308 - 0.623	0.324 - 0.636
MUMEAN	median	22.022	22.120
	[$Q1 - Q3$]	21.925 - 22.105	22.074 - 22.143
F775W_MAG	median	21.284	22.169
	[$Q1 - Q3$]	20.324 - 22.538	21.384 - 23.492

Moreover, according to Parekh et al. (2015) it was determined that galaxies are classified into most relaxed, relaxed and non-relaxed ones based on values of GINI coefficient where the non relaxed (peculiar/most disturbed) galaxies being characterized by $GINI < 0.4$ criterion. It is also described for the most disturbed galaxies that GINI value is small because bright pixels are not compact while equally distributed in the given aperture radius. Accordingly eight non-relaxed galaxies (peculiar) were identified from LT class closer to the cluster core leaving the spiral population near the core to be very small.

For the overall galaxy population, Moran et al. (2007) determined that for 123 matching galaxies within the 1Mpc region, 65.6% were ET while 34.1% being LT. In the same work the morphology was determined for MS0451-0305 galaxy cluster at $z \sim 0.5$ with 52% and 48% being ET and LT, respectively. The galaxy population in our work follows nearly the same trend as what has been on board for cluster studies confirming ET population is greater than the LT population (see Postman et al. 2005 & Moran et al. 2007).

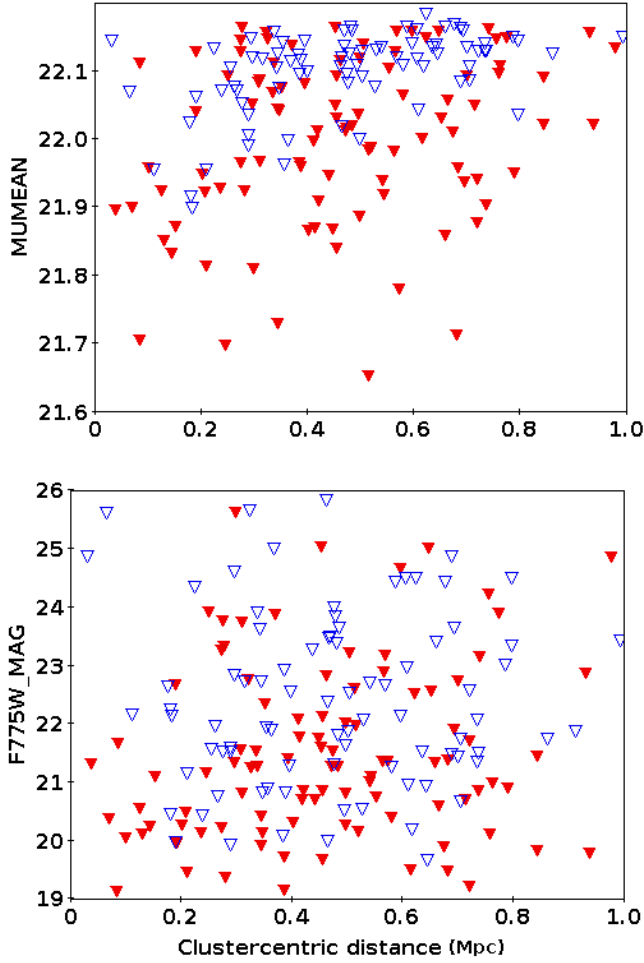


Figure 12. Relation between the surface brightness (top) and F775W magnitude (bottom) with clustercentric distance. For symbols description see Fig. 9.)

As shown in Sec 3.5, out of the 231 galaxies we have 42 % and 36 % galaxies classified as ET and LT, respectively.

5.2 Morphology versus ELGs

Using GLACE survey data, [Sánchez-Portal et al. \(2015\)](#) has presented a catalogue of 174 unique emission line galaxies (ELGs) in our cluster within 4 Mpc clustercentric distance. Accordingly $\sim 37\%$ of the ELGs (64 galaxies) were shown to be AGN (broad line AGN (BLAGN) and narrow line AGN (NLAGN)) whereas $\sim 63\%$ being star forming (SF) galaxies (110 in number). Out of the 174 ELGs, 79 galaxies (52 SFs ($\sim 66\%$) and 27 AGNs ($\sim 34\%$)) were within the clustercentric distance of 1 Mpc (region of our concern). Matching the GLACE result with ours we found 43 ($\sim 54.4\%$) counterparts. Here 26 ELGs had no match in our catalogue may be because [Sánchez-Portal et al. \(2015\)](#) was working only on ELGs but this is not the case of our work. Out of the matching 43 sources, 26 ($\sim 60.5\%$) are SF while the remaining 17 ($\sim 39.5\%$) are AGN. Morphologically comparing the matching ELGs; 11 galaxies ($\sim 26\%$) correspond to ET, 28 galaxies

($\sim 65\%$) belong to LT and the remaining 4 galaxies ($\sim 9\%$) correspond to UD class in our results. More specifically 18 SF galaxies are in LT class where 5 SF galaxies fall in ET while the remaining 3 SF galaxies belong to UD class. Similarly for AGN; LT contributes 10, ET contributes 6 while UD contributes only 1 AGN. This confirms that ELGs (SF as well as AGN) are mostly galaxies rather than ET galaxies.

5.3 Morphological fractions

In Fig. 13 we compared the morphological fraction with both F775W magnitude and clustercentric distance. To compare it with magnitude (left plot of Fig. 13), morphological fraction is computed for each 1 magnitude bin in such a way that a particular class fraction is the ratio of the number of a given class galaxies to the total number of galaxies of all classes within the same bin. This for instance, is given for ET fraction in a given bin as:

$$MAG_ET_{frac} = \frac{\text{number of ETs}}{\text{total number of galaxies}}, \quad (3)$$

where number of ETs \equiv ETs with magnitudes within the range of the bin; total number of galaxies \equiv number of all galaxies (ET+LT+UD) with magnitudes in the same magnitude range.

Once it is computed for all the bins it is plotted against the centre of the bin. It can be seen that the fraction of ET galaxies decreases as a function of increasing magnitude while that of LT galaxies increases up to F775W ~ 22.5 , remaining nearly constant for fainter magnitudes. The median F775W value for ET is determined to be 21.28 and that for LT is 22.16 while that for UD galaxies is 23.20. Hence we can see that the brightest galaxies are most likely to be resolved and classified into ET/LT whereas fainter galaxies could not easily be resolved, significant number of these galaxies are unlikely to be classified then left as UD. For magnitudes where F775W > 24.5 , the number of sources are very small that the statistics is very poor to draw a conclusion.

According to [Fasano et al. \(2012\)](#), the fraction of ET galaxies is high near the centre of a nearby cluster while decreasing as a function of clustercentric distance. The fraction of LT galaxies on the other hand being smaller closer to the core while increasing as a function of clustercentric distance (see also [Zwicky 1942](#); [Dressler 1980](#); [Whitmore et al. 1993](#); [Pintos-Castro et al. 2016](#)). Here to compare with clustercentric distance (right panel of Fig. 13) we compute the morphological fraction in each 0.2 Mpc bin for 0 to 0.6 Mpc, 0.1 Mpc bin for 0.6 to 0.7 Mpc and 0.3 Mpc bin for 0.7 Mpc to 1 Mpc in the same way as in eq. 3. Once it is computed for all the bins it is plotted against the centre of the bin. Results of our current work (see Fig. 11 and the right plot of Fig. 13) confirm that closer to the core, the ET population fraction is higher than the LT fraction, but ET fraction is observed decreasing and LT fraction increasing until the clustercentric distance of ~ 0.3 Mpc. Whereas beyond ~ 0.3 Mpc fractions of both populations continue nearly flat in parallel up to a clustercentric distance; $R \sim 1$ Mpc. For clustercentric distances where $R > 0.7$ Mpc, the number of sources are very small that the statistics is very poor to conclude. We can see in general on Fig. 13 throughout the entire region that the fraction of ET galaxies is consistently higher than the LT fraction and more fraction of galaxies is classified into

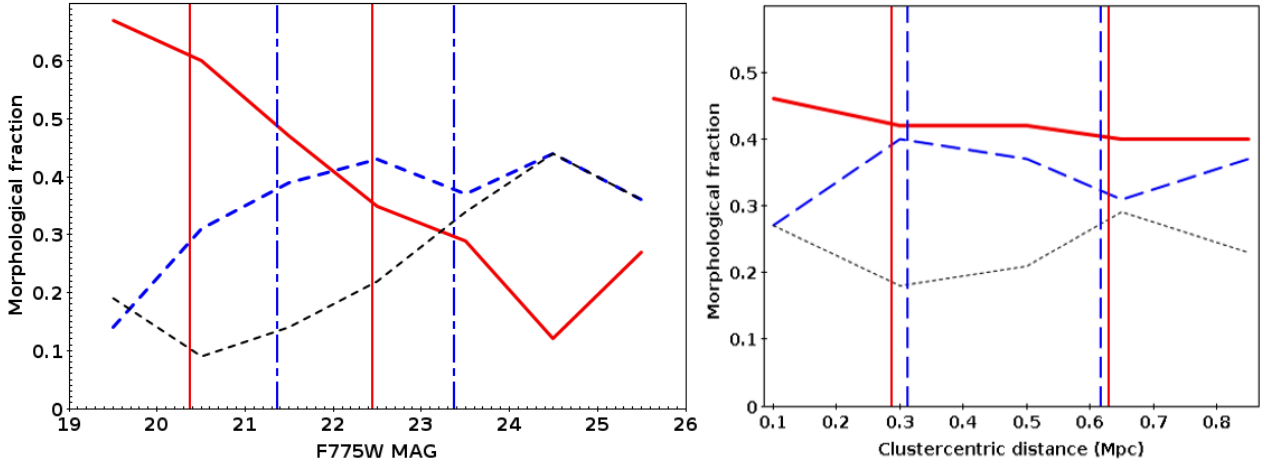


Figure 13. Morphological fractions as a function of F775W (left panel) with a binning size of 1 MAG and as a function of clustercentric distance (right panel) with a binning size of 0.2 Mpc along the x-axis. The thick red plot is for ET fraction, the blue dashed plot for the LT and the black thinner dashed plot for UD fraction. The thick red vertical lines indicate the Q1 & Q3 for ET fraction while the dashed blue vertical lines stand for the Q1 & Q3 of the LT fraction.

ET/LT near the core (lower UD fraction) than in far distances (where higher UD fraction) from the centre. Hence, our results are in a good agreement with previous results.

Moreover, out of the total number of 231 galaxies with in the cluster; 111 have spectroscopically confirmed redshifts while 120 have photometric redshifts. Different trends are observed in morphological fractions throughout the clustercentric distance. It can easily be seen that for galaxy population with spectroscopic redshifts, ET fraction is greater than the LT fraction throughout the region. While for galaxies with photometric redshifts, the LT fraction dominates throughout over the ET fraction.

5.4 Morphology-density relation

An important point to be raised is morphology - density relation. As shown by Hoyle et al. (2012), there is a trend of an increase in the population of ET galaxies towards the cluster centre accompanied by a strong morphology - density relation. Previous studies have already described a high - intermediate - low density regions in a cluster (see Jee et al. 2005; Demarco et al. 2010). Analysing a cluster at $z=0.84$, Nantais et al. (2013) determined that the cluster outskirts (intermediate to low density region) is characterised by higher LT while lower spiral with more peculiar (merging) galaxy population. Whereas a high density region (cluster core) with dominating ET population, few peculiar galaxies and almost devoid of spirals. It has been determined near the cores of clusters that the proportion of ET galaxies is $\sim 47\%$, that is ~ 2.8 times greater than the ET fraction in the field at the same intermediate redshift (see Delgado-Serrano et al. 2010 & Nantais et al. 2013). This is a relationship that holds also for low redshift rich clusters as determined for galaxies with redshift of $z \sim 0.1 - 0.2$ by Fasano et al. (2000). In our case, we were working on the broad classes (ET and LT). While there is no clear classification into peculiar (merging) galaxies and these will be included in our classification either into LT or UD. In our work, the proportion of ET is recorded decreasing as going outwards (decreasing den-

sity) from the cluster core at least up to ~ 0.7 Mpc (see the right plot in Fig. 13). As mentioned previously, after the $R=0.7$ Mpc the number of sources decrease significantly in all three morphological groups, which affects the measured fractions. Moreover, LT population decreases approaching to the cluster core in agreement with existing results.

5.5 Relevance of morphological parameters

In Parekh et al. (2015) while working on galaxy classification into relaxed versus dynamically disturbed system using the data of clusters at different redshifts from Chandra archive, they indicated GINI, M20 and Concentration as very promising parameters for identifying mergers. Accordingly, the criteria set for the most relaxed system is that $GINI > 0.65$, $M20 < -2.0$ and $Concentration > 1.55$. For the most dynamically disturbed (non relaxed) system $GINI < 0.4$, $M20 > -1.4$ and $Concentration < 1$ were set. Intermediate between the two extreme conditions is the mildly disturbed situation. They identified that GINI is the most useful parameter in determining substructure because it does not depend on the exact position of the centre. Our classification was done with six morphological parameters (subsection 3.3) to classify the galaxies into ET and LT. Adapting the criteria from Parekh et al. (2015) for our work, $GINI < 0.4$ gave us 12 galaxies classified into ET/LT (ET=1 (8.3%), LT=11 (91.7%)). These 11 LT galaxies are checked visually to be the most perturbed (non relaxed) galaxies, where $M20 > -1.4$ for 9 galaxies out of the 11 LTs (with $\sim 82\%$ agreement). On the other hand corresponding to $GINI > 0.65$; 58 galaxies were classified into ET/LT (ET=49 (85%), LT=9 (15%)) and are the most relaxed ones accordingly. Hence our result in this aspect is subject to 85% agreement with previous works (amount of ETs). But in our work, $M20 < -2.0$ is too small to be used while it is better to take M20 cut off for the most relaxed galaxies to be $\lesssim -1.8$ to establish an accuracy of at least 79%. Moreover, since concentration parameters are defined as in subsection 3.3, from our results the cut off values of $CABR < 0.2$ and

CCON < 7.0 can be used for the most perturbed galaxies with $\sim 91\%$ agreement while CABR > 0.45 and CCON > 7.5 can segregate about $\sim 94\%$ of the most relaxed galaxy population. Therefore with this cut off limits, CCON and CABR parameters could also be equally important parameters as GINI and M20 for morphological classification of galaxies.

5.6 Morphological parameters vs. clustercentric distance

In this work for the first time, we studied the properties of different morphological parameters in relation to the clustercentric distance (R). In Fig. 14 we showed how GINI, ELLIP, M20, CABR, ASYM and CCON change with R for ET and LT galaxies. In general, we do not find any clear trend in case of ASYM, CCON and ELLIP with R. In case of GINI, CABR and M20 a slight trend is observed of decreasing GINI and CABR showing and increasing M20 moment of light, suggesting that as going outwards from the cluster centre the light concentration decreases. However, much better statistics are needed to confirm this result. As shown in the right plot of Fig. 13 for ET class galaxies, the median and [Q1 - Q3] range of R being lower on average than LT, and this can be explained against each parameter. This is accompanied by higher values of GINI, CCON and CABR while lower values of ELLIP, M20 and values about zero for ASYM for ET galaxies. Whereas for LT galaxies, the median and [Q1 - Q3] range of R is slightly higher on average than ET galaxies. This can be seen from the plot describing morphological fraction in Fig. 13. It can also be seen that GINI value slightly decreases as a function of increasing R for LT galaxies. Similar trend is observed from the plot of CABR versus R but very slow decrease for both classes in this case. For other parameters the values almost remain stagnant with R.

6 CONCLUSIONS

In this work as part of a complete morphological study of the cluster ZwCl0024+1652 at an intermediate redshift $z \sim 0.4$, we presented a broad classification of member galaxies with available redshifts within the clustercentric distance of 1 Mpc using the HST/ACS image. We have classified galaxies up to the I - band magnitude of 26. By running galSVM code on a sample of 255 galaxies, 6 morphological parameters were measured and classification was provided for 231 galaxies. Of these, 111 have spectroscopic and 120 photometric redshift measurements. From our classification and analysis we have drawn the following conclusions:

- Out of all the 231 galaxies 97 ($\sim 42\%$) were classified as ET, 83 ($\sim 36\%$) as LT and 51 ($\sim 22\%$) stayed unclassified. If we take the well classified galaxies (180 in number); 97 ($\sim 54\%$) were classified as ET whereas 83 ($\sim 46\%$) fall into an LT class.
- Comparing with the visual classification results in Moran et al. (2007) we have classified 53 galaxies matching with their previous visual morphologies, 6 galaxies classified to different classes and 121 new sources which didn't have any reported morphological classification within ~ 1 Mpc radius are newly classified in our work. Therefore this work

work gives the most complete and largest morphological catalogue available up to now for our galaxy cluster.

- Moreover, our comparison with the existing visual classification of Moran et al. (2007) is in a good agreement of 81%. Hence, applying galSVM for morphological classification can be taken as a reliable technique to be used even for a large sample.

- We have tested that ET and LT galaxies follow the expected distributions for different standard morphological diagrams, colour - colour and colour - magnitude diagrams.

- The ET morphological fraction is higher near the cluster core decreasing outwards with LT fraction being lower at core increasing outwards. Throughout the region of 1 Mpc radius, the fraction of ET galaxies is consistently greater than the LT fraction for our cluster in the region of our concern (R out to 1 Mpc). Hence, the ET/LT fraction in the cluster is in agreement with previous studies.

- Morphological fractions in our galaxy cluster at $z \sim 0.4$ evolves with magnitude in such a way that ET fraction dominates in the brightest magnitude limit decreasing towards the fainter end while the LT fraction increases as magnitude goes fainter.

- We compared our results with Sánchez-Portal et al. (2015) and found 43 ELG counterparts. As a result out of these counterparts, 11 galaxies ($\sim 26\%$) correspond to ET while 28 galaxies ($\sim 65\%$) were found to belong to LT. with the remaining 4 galaxies ($\sim 9\%$) stayed unclassified in our work. Moreover with the star forming ELGs; 18 SF galaxies are LT, 5 SF galaxies fall in ET and the remaining 3 SF galaxies belong to UD class. Similarly for AGN; LT contributes 10, ET contributes 6 while UD contributes only 1 AGN. Hence, in general we deduce that ELGs are more of LT in morphology than ET.

- We have analysed the morphological parameters as a function of clustercentric distance out to 1 Mpc for the first time. In general we do not find any clear trend, however better statistics would be valuable in future studies to revise the change of galaxy light concentration with R.

This work contributes significantly in the area of studies related to evolution of galaxies in clusters involving morphological classification, and provides the most complete morphological catalogue of ZwCl0024+1652. In our future studies within the GLACE survey, we are planning to compare morphological properties with metallicities, star formation, and AGN contribution using the tunable filters data. Finally, a complete morphological catalogue that resulted from our work can be accessed with an electronic version of this paper. The first seven rows and the descriptions for all the columns are presented as an appendix in this paper.

ACKNOWLEDGEMENTS

We acknowledge the anonymous referee for helpful comments and valuable suggestions that have significantly contributed to improve the paper. We also thank the Ethiopian Space Science and Technology Institute (ESSTI) under the Ethiopian Ministry of Innovation and Technology (MOIT) for all the financial and technical supports. ZBA specially acknowledges Joint ALMA Observatory (JAO); ESO - ALMA at Santiago, Chile for giving financial support and working space while working with M. Sanchez-Portal on the first

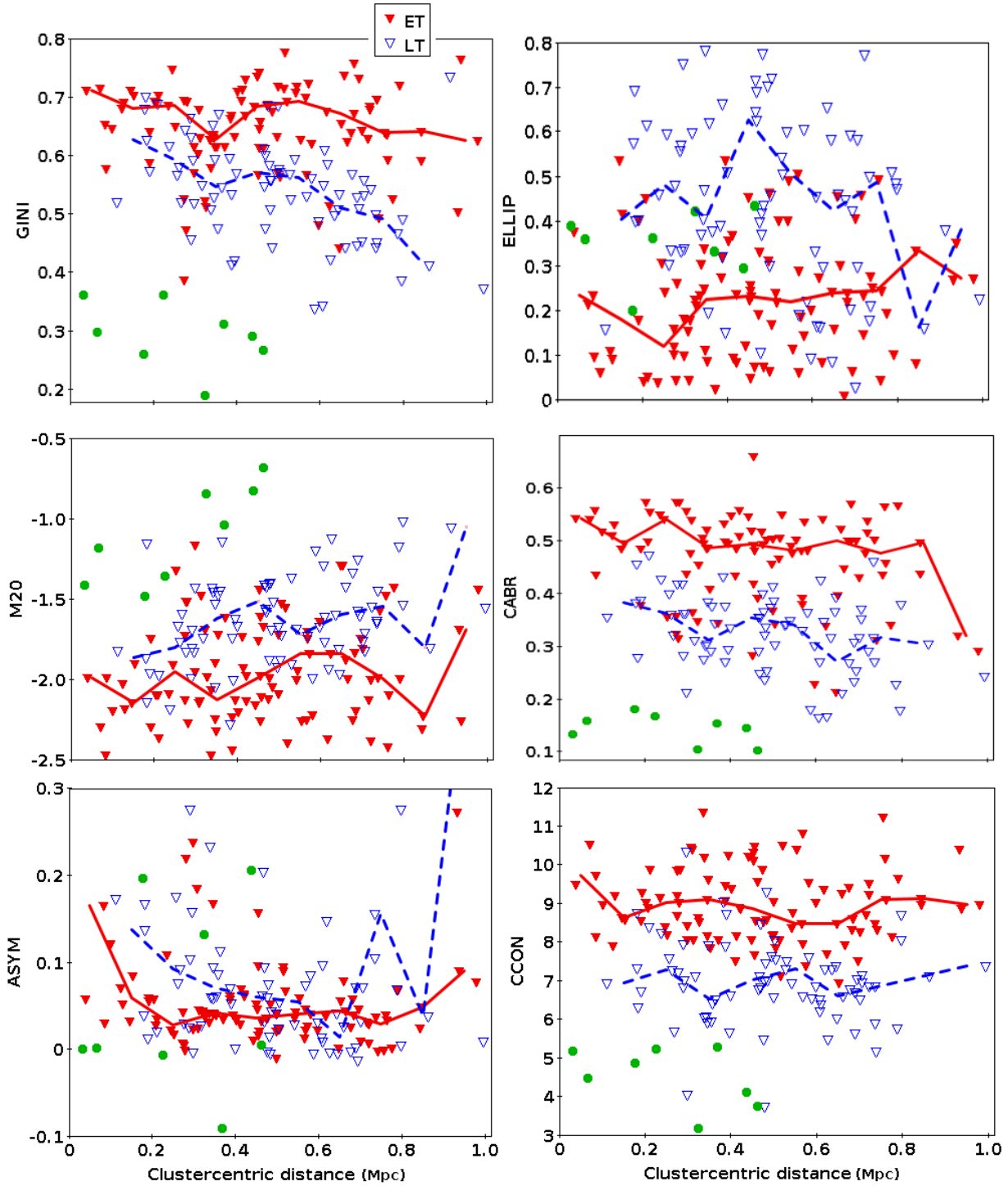


Figure 14. From top to bottom, and from left to right: Relation between the GINI, ellipticity, M20 moment of light, CABR concentration index, asymmetry, and CCON concentration index and distance from the cluster centre. In all plots red solid triangles stand for ET, and blue open triangles for LT galaxies. The disturbed (merging) galaxies selected from LT based on GINI < 0.4 criteria are indicated with green dots (solid circles). Median values of each parameter with clustercentric distance are shown with the red solid and blue dashed lines of ET and LT galaxies, respectively.

phase of the paper. Moreover ZBA acknowledges Kotebe Metropolitan University for granting a study leave and giving material supports. MP and SBT acknowledge financial support from the Ethiopian Space Science and Technology Institute (ESSTI) under the Ethiopian Ministry of Innovation and Technology (MoIT). MP also acknowledges support from the Spanish MINECO under projects AYA2013-42227-P and AYA2016-76682-C3-1-P, and from the State Agency for Research of the Spanish MCIU through the “Center of Excellence Severo Ochoa” award for the Instituto de Astrofísica de Andalucía (SEV-2017-0709). In this work, we made use of Virtual Observatory Tool for Operations on Catalogues And Tables (TOPCAT) and IRAF. IRAF is distributed by the National Optical Astronomy Observatories, which are operated by the Association of Universities for Research in Astronomy, Inc., under cooperative agreement with the National Science Foundation. We also used ACS/HST data based on observations made with the NASA/ESA HST, and obtained from the Hubble Legacy Archive, which is a collaboration between the Space Telescope Science Institute (STScI/NASA), the Space Telescope European Coordinating Facility (ST-ECF/ESA) and the Canadian Astronomy Data centre (CADM/NRC/CSA). This work was supported by the Spanish Ministry of Economy and Competitiveness (MINECO) under the grants AYA2014-58861-C3-2-P, AYA2014-58861-C3-3-P, AYA2017-88007-C3-1-P and AYA2017-88007-C3-2-P.

REFERENCES

- Abazajian, K., et al. 2009, *ApJS*, 182, 543
- Abraham, R. G., Valdes, F., Yee, H. K. C., & van den Bergh, S., 1994, *ApJ*, 432, 75
- Abraham, R. G., van den Bergh, S., Glazebrook, K., et al., 1996, *ApJS*, 107, 1
- Abraham, R. G., van den Bergh, S., & Nair, P., 2003, *ApJ*, 588, 218
- Aniyan, A. K. & Thorat, K., 2017, *ApJS*, 230:20
- Ascaso B., et al., 2009, *A&A*, 506, 1082
- Balogh, M. L., Schade, D., Morris, S. L., et al. 1998, *ApJ*, 504, L75
- Banerji, M., et al. 2010, *MNRAS*, 406, 342
- Barrena R., Girardi M., Boschin W., Mardirossian F., 2012, *A&A*, 540, A90
- Bell, E. F., McIntosh, D. H., Katz, N., & Weinberg, M. D. 2003, *ApJS*, 149, 289
- Bershady M. A., Jangren A., & Conselice C. J., 2000, *AJ*, 119, 2645
- Bertin, E. & Arnouts, S., 1996, *Astronomy & Astrophysics Supplement Series*, 117, 393
- Broadhurst, T., et al., 2000, *ApJ*, 534, L15
- Buitrago, F., et al., 2013, *MNRAS*, 428, 1460
- Butcher, H. & Oemler, A., 1978, *ApJ*, 219,18
- Butcher, H. & Oemler, Jr., A. 1984, *ApJ*, 285, 426
- Cassata P., et al., 2007, *ApJS*, 172, 270
- Chang, C. C. & Lin, C. J., 2011, *ACM Transactions on Intelligent Systems & Technology*, Volume 2, Article 27 Software available at <http://www.csie.ntu.edu.tw/~cjlin/libsvm/>
- Conselice, C. J., Bershady, M. A., Dickinson, M., & Papovich, C., 2000, *ApJ*, 529, 886
- Conselice C. J., Bershady M. A., Dickinson M., & Papovich C., 2003, *AJ*, 126, 1183
- Cooper M. C. et al., 2012, *MNRAS*, 419, 3018
- De Lucia G. et al., 2007, *MNRAS*, 374, 809
- Delgado-Serrano, R., Hammer, F., Yang, Y. B., et al. 2010, *A&A*, 509, A78
- Demarco, R., Gobat, R., Rosati, P., et al. 2010, *ApJ*, 725, 1252
- Dieleman, S., Willett, K. W., & Dambre, J., 2015, *MNRAS*, 450, 1441
- Dressler, A., 1980, *ApJ*, 236,351
- Dressler, A. & Gunn, J. E., 1982, *ApJ*, 263,533
- Dressler, A., Gunn, J. E., & Schneider, D. P., 1985, *ApJ*, 294,70
- Dressler A. et al., 1997, *ApJ*, 490, 577
- Domínguez, S., et al., 2018, *MNRAS*, 476, 3661
- Fasano G., et al., 2000, *ApJ*, 542, 673
- Fasano G. et al., 2012, *MNRAS*, 420,926
- Fairley B. W., et al., 2002, *MNRAS*, 330, 755
- Geach J. E., et al., 2009, *AJ*, 691, 783
- Gunn, J. E. & Oke, J. B., 1975, *ApJ*, 195,255
- Haines, C. P., Smith, G. P., Egami, E., et al. 2009, *ApJ*, 704, 126
- Holden B. P. et al., 2007, *ApJ*, 670, 190
- Hoyle B. P. et al., 2012, *MNRAS*, 423, 3478
- Huertas-Company, M., Rouan, D., Soucail, G., et al. 2007, *A&A*, 468, 937
- Huertas-Company, M., Rouan, D., Tasca, L., Soucail, G., & Le Fevre, O., 2008, *A&A*, 478, 971
- Huertas-Company, M., Tasca, L., Rouan. D., et al. 2009, *A&A*, 497, 743
- Huertas-Company, M., Aguerri, J. A. L., Tresse, L., et al., 2010, *A&A*, 515, A3
- Huertas-Company, M., Aguerri, J. A. L., Bernardi, M., Mei, S., & Sanchez Almeida, J. 2011, *A&A*, 525, 157
- Huertas-Company, M., Mei, S., et al., 2013, *MNRAS*, 428, 1715
- Huertas-Company, M., et al., 2015, *ApJS*, 221:8
- Humason, M. L. & Sandage, A., 1957, in *Carnegie Yearbook 1956* (Carnegie Institution of Washington), P61
- Jee, M. J., White, R. L., Benitez, N., et al. 2005, *ApJ*, 618, 46
- Kauffmann G., White S. D. M., Heckman T. M., et al. 2004, *MNRAS*, 353, 713
- Kartaltepe J. S., et al. 2012, *ApJ*, 757, 23
- Kartaltepe J. S., et al. 2015, *ApJS*, 221:11
- Kneib, J-P., et al. 2003, *ApJ*, 591, 53
- Kocevski, D. D., et al. 2012, *ApJ*, 744, 148
- Kuminski, E., et al. 2014, *PASP*, 126, 959
- Kuminski, E. & Shamir, L., 2016, *ApJS*, 223:20
- Lintott, C. J., et al. 2008, *MNRAS*, 389, 1179
- Lintott, C. J., et al. 2011, *MNRAS*, 410, 166
- Lotz, J. M., Primack, J., & Madau, P., 2004, *AJ*, 128, 163
- Lukic, V., et al., 2018, *MNRAS*, 476, 246
- Martini, P., Miller, E. D., Brodwin, M., et al. 2013, *ApJ*, 768, 1
- Mei S. et al., 2012, *ApJ*, 754, 141
- Melbourne, J., Phillips, A. C., et al., 2007, *ApJ*, 660, 81
- Moles, M., et al. 2008, *AJ*, 136, 1325
- Moran, S. M., Ellis, R. S., Teu, T., et al. 2005, *APJ*, 634, 977
- Moran, S. M., Ellis, R. S., Teu, T., et al. 2007, *APJ*, 671, 1503
- Morrison, G., et al. 1997, *AAS*, 29, 1399
- Nantais, J. B., Flores, H., Demarco, R., et al. 2013, *A&A*, 555, A5
- Nair P. B., & Abraham R., 2010, *ApJS*, 186, 427
- Natarajan P., et al., 2009, *ApJ*, 693, 970
- Nilo Castellón J. L. et al., 2014, *MNRAS*, 437, 2607
- Oke, J. B., & Gunn, J. E., 2015, *A&A*, 575, A127
- Parekh, V., et al. 2013, *ApJ*, 266, 713
- Peng, C. Y., Ho, L. C., Impey, C. D., & Rix, H. W., 2002, *AJ*, 124, 266
- Peng C. Y., Ho L. C., Impey C. D., Rix H.-W., 2010, *AJ*, 139, 2097
- Pintos-Castro, I., Sánchez-Portal M., et al. 2013, *A&A*, 558, A100
- Pintos-Castro, I., Pović, M., et al. 2016, *A&A*, Accepted
- Postman M., Geller M. J., 1984, *ApJ*, 281, 95
- Postman, M., Franx, M., Cross, N. J. G., et al. 2005, *ApJ*, 623, 721

- Pović M., Sánchez-Portal M., et al. 2009, *ApJ*, 706, 810
Pović M., Sánchez-Portal M., et al. 2012, *A&A*, 541, A118
Pović M., Huertas-Company M., et al. 2013, *MNRAS*, 435, 3444
Pović M., Márquez I., et al. 2015, *MNRAS*, 453, 1644
Quadri R. F., Williams R. J., Franx M. & Hildebrandt H. 2012, *ApJ*, 744, 88
Reynolds, J. H., 1920, *MNRAS*, 80, 746
Sánchez-Portal M., Pintos-Castro I., et al. 2015, *A&A*, 578, A30
Scarlata, C., et al., 2007, *ApJS*, 172, 406
Schawinski, K., et al., 2014, *MNRAS*, 440, 889
Schneider, D. P., Dressler, A., & Gunn, J. E., 1986, *AJ*, 92, 523
Sérsic, J. L., 1963, *Boletín de la Asociación Argentina de Astronomía*, 6, 41
Simard, L., Willmer, C. N. A., Vogt, N. P., et al. 2002, *ApJS*, 142, 1
Simard, L., et al. 2009, *A&A*, 508, 1141
Simard, L., et al. 2011, *ApJSS*, 196, 11
Simmons, B. D., et al., 2017, *MNRAS*, 464, 4420
Smith, G. P., Treu, T., Ellis, R. S., Moran, S. M., & Dressler, A. 2005, *ApJ*, 620, 78
Tarsitano, F., et al., 2018, *MNRAS*, 481, 2018
Tasca, L. A. M., et al. 2009, *A&A*, 503, 379
The DES Collaboration 2016, *MNRAS*, 460, 1270
Tran, K.-V. H., Papovich, C., Saintonge, A., et al. 2010, *ApJ*, 719, L126
Treu, T., Ellis, R. S., Kneib, J., et al. 2003, *APJ*, 591, 53
Weisstein, Eric W. 2012, "Spherical Trigonometry." From MathWorld – A Wolfram Web Resource. <http://mathworld.wolfram.com/SphericalTrigonometry.html>, last visited on 07/05/2018
Wetzel A. R., Tinker J. L., Conroy C., 2012, *MNRAS*, 424, 232
Whitmore, B. C., Gilmore, D. M., & Jones, C. 1993, *ApJ*, 407, 489
Willett, K. W., et al. 2013, *MNRAS*, 435, 2835
Willett, K. W., et al. 2017, *MNRAS*, 464, 4176
Woo J. et al., 2013, *MNRAS*, 428, 3306
Ziparo, F., Popesso, P., Finoguenov, A., et al. 2014, *MNRAS*, 437, 458
Zwicky, I. F., 1942, *ApJ*, 95, 555

APPENDIX A: THE COMPREHENSIVE MORPHOLOGICAL CATALOGUE OF GALAXIES IN ZWCL0024+1652 CLUSTER AT $Z \sim 0.4$

A complete morphological catalogue of 231 sources (111 with spectroscopically confirmed redshifts while 120 with photometric redshifts) is presented in this work. This is the most comprehensive catalogue containing the morphological classes of galaxies in ZwCl0024+1652 cluster; classified with galSVM technique. The entire catalogue comprises of a table of 231 rows standing for sources (galaxies) and 34 columns with respective parameter for each row. In this catalogue, the morphological class is identified for 180 galaxies but the remaining 51 galaxies are marked undecided in terms of the morphological class. In addition to parameters measured in this work, SExtractor measured photometric data and results from previous works (Treu et al. 2003; Moran et al. 2005; Moran et al. 2007 and Sánchez-Portal et al. 2015) is also included in this catalogue. The followings are descriptions of each column of the entire catalogue.

Column 1 ... Source index (galaxy number);

Column 2 ... HST identification number of the galaxy (99.0 if not available);

Column 1 ... Source index (galaxy number);

Column 2 ... HST identification number of the galaxy (99.0 if not available);

Column 3 ... Right Ascension in decimal degrees (J2000);

Column 4 ... Declination in decimal degrees (J2000);

Column 5 ... Ellipticity of the galaxy measured by SExtractor;

Column 6 ... MUEAN value for the galaxy measured by SExtractor;

Column 7 ... Asymmetry index measured by galSVM (described in subsection 3.3);

Column 8 ... Abraham concentration index measured by galSVM (described in subsection 3.3);

Column 9 ... GINI coefficient measured by galSVM (described in subsection 3.3);

Column 10 ... M20 moment of light index measured by galSVM (described in subsection 3.3);

Column 11 ... Bershadsky-Concelice concentration index measured by galSVM (described in subsection 3.3);

Column 12 ... MAG_AUTO (F775W) (we measured it by SExtractor for each source);

Column 13 ... Uncertainty in MAG_AUTO (F775W) measured by sextractor for each source;

Column 14 ... Redshift values for each galaxy from the public data of ZwCl0024+1652 master catalogue generated by a team working on a "A Wide Field Survey of Two $z = 0.5$ Galaxy Clusters" (see Treu et al. 2003 and Moran et al. 2005).

Column 15... Zsource (=6 from DEIMOS, 1-5: other spectroscopic sources (see Moran et al. 2007) 7=secure photo-z (see Smith et al. 2005, 8=fairly unreliable photo-z (fewer bands,fainter);

Column 16 ... Distance of the galaxy from the centre of the cluster (clustercentric distance) measured in Mpc;

Column 17 ... The final probability computed taking the uncertainty (error) into account (used for morphologically classifying the galaxies in current work);

Column 18 ... The final morphological class (Early_Type

(ET), Late-Type (LT) or Undecided (UD)) based on the final probability value

Column 19 ... Visual morphology as given in [Moran et al. \(2007\)](#); = -99.9 if not available;

Column 20 ... Emission Line Galaxy (ELG) type adapted from [Sánchez-Portal et al. \(2015\)](#); = -99.9 if not available;

Columns 21 - Column 34 ... SExtractor measured photometric data (MAG_AUTOs and errors) for the galaxies taken from public data of ZwCl0024+1652 master catalogue (see [Treu et al. 2003](#) and [Moran et al. 2005](#)); = 99. if not available, = -99.9 if all values not measured.

Part of the catalogue (the column values for the first seven sources) is presented in Table A1. For sample illustration, the first 7 rows of the electronic version of the catalogue with values of the columns (all the parameters) are presented here.

This paper has been typeset from a $\text{\TeX}/\text{\LaTeX}$ file prepared by the author.

Table A1. Part of the Morphological Catalogue of galaxies in ZwCl0024+1652 Cluster (Full catalogue is available online)

NUMBER	HST_ID	RA (deg)	DEC (deg)	ELLIP	MUMEAN
ASYM	CABR	GINI	M20	CCON	F775W_Mag
F775W_ERR	Redshift	Zsource	R(Mpc)	PROBA_FINAL	GALAXY_CLASS
Visual_Morpho	ELG_Type	B_AUTO	V_AUTO	R_AUTO	LAUTO
J_AUTO	K_AUTO	F814W_AUTO	B_ERR	V_ERR	R_ERR
LERR	J.ERR	K.ERR	F814W_ERR		
1	80.0	6.62029	17.13273	.2272	22.1522
.0087	.2443	.3740	-1.5537	7.3720	23.4480
.3906	.3810	8	.9763	.3049	LT
-99.9	-99.9	25.7701	24.9023	23.7896	23.0985
21.5017	19.9099	22.7271	.1837	.1923	.0870
.0974	99.	99.	.0268		
2	99.0	6.65543	17.13758	.5847	22.1088
.5657	.3714	.5321	-1.8222	6.9793	20.7002
.1101	.3940	1	.6997	.1017	LT
-99.9	-99.9	23.4553	22.4472	21.1820	20.3412
18.9132	17.3511	99.0	.0251	.0224	.0090
.0086	.0551	.0561	99.		
3	116.0	6.63273	17.13629	.2521	22.1632
-.0019	.3118	.4927	-1.5734	8.3250	23.1702
.3437	.3660	8	.7356	.7600	ET
-99.9	-99.9	25.2051	24.4749	23.4430	22.9775
21.4379	19.8460	22.7281	.1164	.1378	.0672
.0924	99.	99.	.0120		
4	126.0	6.64078	17.13619	.2470	22.1618
.0642	.2593	.4668	-1.4197	7.7667	24.5245
.6413	.3780	8	.6845	.5944	UD
-99.9	-99.9	26.9703	26.0467	25.7980	23.5168
21.5139	19.9220	23.8584	99.	99.	99.
.1415	99.	99.	.0234		
5	9.0	6.66708	17.13923	.3327	22.0930
.0482	.4381	.5917	-2.2275	8.9588	21.4544
.1559	.3999	6	.8261	.7411	ET
S0	NLAGN	24.1371	22.8917	21.7965	21.1522
20.1556	18.8312	20.9172	.0398	.0291	.0136
.0155	.1482	.1887	.0079		
6	99.0	6.65664	17.13732	.4107	22.1440
-.0049	.3036	.5818	-1.3960	10.8122	24.0350
.5118	.4470	8	.7183	.5125	UD
-99.9	-99.9	25.2620	25.2038	24.0649	23.5652
21.4067	19.8148	99.0	.1260	.2766	.1221
.1632	99.	99.	99.		
7	58.0	6.64736	17.13850	.0849	22.1506
-.1024	.3391	.5138	-1.8383	7.7022	22.5379
.2568	.3840	7	.6226	.6945	ET
-99.9	-99.9	24.9017	24.1310	23.2602	22.2188
21.5017	19.9099	22.0129	.0836	.0950	.0537
.0435	99.	99.	.0074		